SEISMIC ROBUSTNESS OF SELF-CENTERING BRACED FRAMES SUFFERING TENDON FAILURE

Yiwei Ping[1], Cheng Fang[1*], Yiyi Chen[1], Michael C H Yam[2]

[1] State Key Laboratory of Disaster Reduction in Civil Engineering & Department of Structural Engineering, Tongji University, Shanghai 200092, China

[2] Department of Building & Real Estate, The Hong Kong Polytechnic University, Hung Hom, Kowloon, Hong Kong, China

*Corresponding author: Tel: +86 21 65982926; Fax: +86 21 65984976, Email: chengfang@tongji.edu.cn.

Abstract: This paper comprehensively discusses the behavior and failure risk of self-centering braced frames (SCBFs) suffering tendon fracture. The fundamental mechanism of tendon failure in self-centering braces (SCBs) is first introduced, followed by the design and analysis of a series of prototype buildings with different tendon materials and brace configurations. Assuming a normal distribution of tendon fracture strain, the dynamic behavior of the frames is then assessed by a suite of ground motion records, covering both far-field and near-fault ones. The collapse and residual deformation fragilities of the frames are further evaluated, and the study ends with a risk assessment considering a 50-year service period. Among other findings, the study indicates that tendon fracture tends to increase the peak inter-story drift, especially for the structure with smaller tendon fracture strains. Tendon fracture also compromises the self-centering capability significantly, although there is no obvious statistical correlation between tendon fracture and the peak floor acceleration. The probability of collapse and that of exceedance of certain residual drift both increase evidently when tendon fracture is considered. The failure probabilities are closely related to the available deformability of the SCBs, where dual-core SCBs show less sensitivity to tendon fracture. The probability of collapse of the considered frames over 50 years of service increases from 1.25~2.12% to 3.58~6.52% when tendon fracture is considered. Considering a residual drift threshold of 0.5%, the probability of exceedance of the same structures over the same life span increases from 1.78~3.54% to 5.46~9.71%.

KEYWORDS

Self-centering brace, seismic robustness, tendon fracture, fragility analysis, risk assessment.

INTRODUCTION

While seismic design philosophy has been advancing over the past decades, earthquakes still bring huge functional and economic loss to modern society. For example, in the 2011 Christchurch earthquake, hundreds of buildings which did not collapse were demolished because of unacceptable residual deformation and damage[1]. A post-earthquake survey suggested that a building is deemed irreparable when its residual inter-story drift exceeds 0.5%[2]. For typical steel frames, however, the residual inter-story drift is usually between 2% and 4% following a large magnitude earthquake[3]. As public awareness of structural resilience has significantly risen, the community of seismic engineers starts to seriously consider residual deformation as a critical seismic performance metric. An emerging class of structural systems, namely, self-centering structures, has received extensive research interests[4-16]. Among the various solutions, self-centering brace (SCB) with post-tension (PT) tendons has become the most popular one because it is shop prefabricated, easy to install, free from slab restraints (in contrast to PT connections), and has high commercialization value.

However, one major concern for the existing SCB design is the limited ductility which is attributed to the small elastic strain of the PT tendons. The "first-generation" SCB was that with one pair of paralleled tubes (single-core), where the PT tendons are affixed to the two end plates and the deformation capacity of the brace is determined by the effective length and the available elastic strain of the individual PT tendons[17,18]. The concept was later extended to double the elongation capacity by utilizing serial deformations of PT tendons with a new telescoping or dual-core configuration[19-23]. In these studies, the materials used for the PT tendons include Technora (a commercialized aramid), high-strength steel, as well as E-glass, T-700, and basalt fiber reinforced polymers (BFRP). The available inter-story drift observed from most of these investigations generally ranges between 2~2.5% before failure of the PT tendons, and this level of ductility supply could be insufficient for steel frames under strong earthquakes. Other researchers have employed shape memory alloys (SMAs) to provide significantly increased deformation capacity and extra energy dissipation thanks to the superelastic effect[24-33], although the temperature dependency and cost issues need to be carefully addressed. A recent study conducted by Chen et al.[34] found that anchor slippage was the main failure mode for SCBs with SMA tendons.

Apart from the PT tendon-based solution, new SCB designs with compressive springs have been emerging[34-38]. Xu et al.[36] conducted a series of tests on an alternative type of SCB with disc springs. It was found that the specimens experienced evident residual deformation when the inner tube yielded, and finally failed in fracture of the inner tube due to stress concentration near its openings. A subsequent study conducted by the same authors[37] showed that the brace failed in overall buckling under compression when the axial deformation ratio exceeded 2.0%. Kitayama and Constantinou[38] developed a new fluidic self-centering device and highlighted through pushover analysis the influence of device failure on the lateral load resistance of the structure. It was warned that when device failure initially occurs, inelastic deformation may be concentrated at that particular story.

The above studies revealed various possible failure modes, including rupture/yielding of PT tendons, slippage of anchorage, and failure of other force transferring components, of the existing SCBs. These failure modes happen alone or successively, and can be either accidental (unexpected) or predictable. Regardless of the nature of the failure, the function of the brace is inevitably compromised, causing a significant violation of the intended load transfer path against the lateral load. The loss of the braces may also lead to a soft story mechanism[38], which considerably jeopardizes the safety of the structure. Moreover, the self-centering capability is no longer guaranteed once the braces quit working, and the damaged SCBs are indeed difficult to repair and therefore need to be replaced after the earthquake. This slows down the recovery process and puts the structure in danger during aftershocks.

The phenomenon of "loss of brace function" is in a sense similar to the concept of "loss of column" in structural robustness assessment. Robustness indicates the ability of a structure subject to extreme loads, such as blast, to resist the progression of local damage to global failure, i.e., progressive collapse. Similarly, one may define "seismic robustness" as the ability of the structure to prevent collapse during strong earthquakes when critical lateral load resisting members (e.g., braces) suddenly fail, as well as the ability to eliminate the residual deformation as far as self-centering frames are concerned. Seismic robustness needs to receive sufficient attention among SCB developers and structural engineers because the loss of SCB function is not a low-probability event especially under aggressive events such as large-magnitude and pulse-like near-fault earthquakes. It is also reminded that the peak deformation of self-centering structures is often amplified compared with conventional yielding systems (e.g., BRBF) because of the decreased energy dissipation and the associated high-mode effect[39,40].

To the authors' best knowledge, however, the influence of the failure of SCBs on the system-level performance has been rarely investigated. One may argue that the risk of SCB failure is remote if the maximum inter-story drift is strictly controlled under the design earthquake, but this is in fact difficult to guarantee given the large uncertainty of the seismic effect, not to mention the pulse-like near-fault ground motions that cause much higher structural demands[39]. In addition, as part of the decision-making process, the owner and other stakeholders are interested in understanding the performance/risk of the self-centering frame beyond the design earthquake[41]. Moreover, the influence of brace failure on the residual inter-story drift and floor acceleration responses are still unclear, noting that the latter was largely responsible for the injuries, fatalities, repair costs and disruption time in the past major earthquakes[42,43].

This paper discusses the behavior of self-centering braced frames (SCBFs) subjected to the risk of tendon failure. In the following discussions, the considered type of SCB and the associated fracture strain of the PT tendons are first introduced, followed by a detailed discussion of the fundamental mechanism of tendon failure in SCBs. A series of prototype buildings are then designed, considering different tendon materials and brace configurations. These structures are subsequently assessed in terms of peak/residual inter-story drift ratio and peak floor acceleration responses by a suite of ground motion records, covering both far-field and near-fault ones. Finally, the performance of the SCBFs is probabilistically assessed through collapse and residual deformation fragility analysis, and a risk assessment is conducted considering a 50-year service period.

BASIC CHARACTERISTICS OF SCBS

Considered SCB type

While there are various types of SCBs developed by different research groups, the present study focuses on the PT-tendon-based configuration, which is perhaps one of the most widely studied SCB types in the community[17-23]. The PT tendons provide the self-centering capability, and energy dissipation is typically provided by additional friction devices. As shown in Figure 1, both single-core and dual-core configurations are considered, where the latter ideally offers the deformation capacity twice that of the former if the prestress level is the same. Another noticeable difference is that the "post-yield" stiffness of the dual-core SCB should be half of that of its single-

core counterpart because of the doubled elongation. The detailed design and manufacture of the considered SCBs can be found elsewhere[17-21] which are not repeated here.

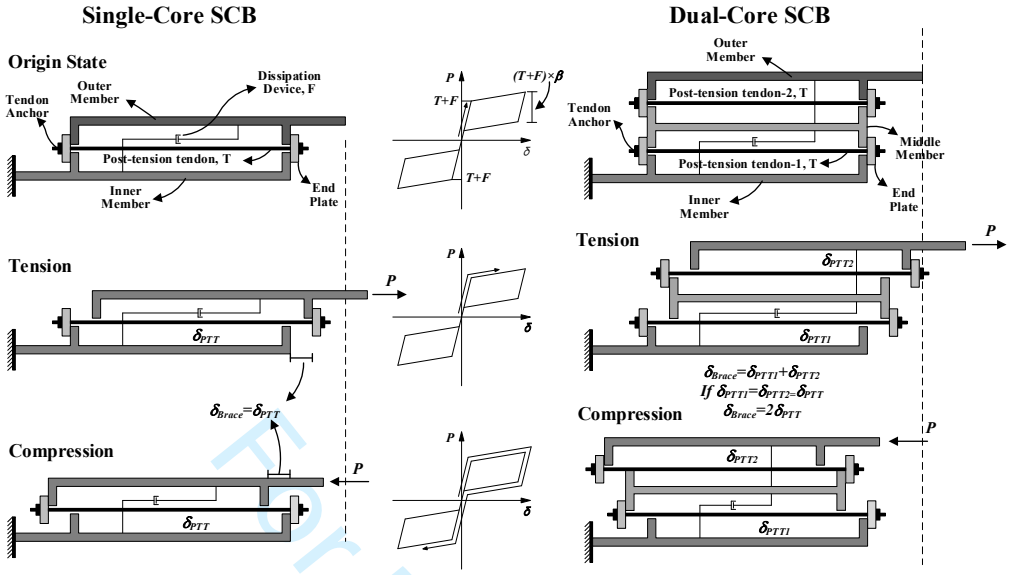

Figure 1 Schematic illustration of working mechanism of single- and dual-core SCBs

Fracture strain of PT tendons

FRP composite tendons are the mainstream self-centering elements used in SCBs because of the relatively large elastic strain (compared with steel tendons). Table 1 gives the basic properties of various types of FRP composite tendons reported by other researchers[44-46]. Among these, Technora is a commercialized aramid which has the largest fracture strain. Basalt FRP (BFRP) and Glass FRP (GFRP) are also popular candidates which have a lower cost than Technora. Carbon FRP (CFRP) has the smallest fracture strain and is therefore less considered in the SCBs. In the present study, Technora and BFRP are selected as the representative PT-tendon materials, which are designated with Material-A (MA) and Material-B (MB), respectively, for ease of reference. According to the available material test reports, the mean fracture strains of MA and MB tendons with a typical diameter of 12~16 mm are 3.8% and 2.4%, respectively[44,45]. The failure process is often abrupt and brittle. The existing studies also showed that the fracture strain of the two materials generally follows a normal distribution, with a standard deviation of 0.15 and 0.2, respectively. Such information is useful when considering the randomness of the tendon fracture behavior in the analysis, as discussed later.

Table 1 Basic properties of common FRP tendons – typical values

Property		Technora (MA)[44]	BFRP (MB)[45]	CFRP[46]	GFRP[46]
Basic property	Density (g/cm^3)	1.30	2.65	2.00	2.62
	Tensile Strength (GPa)	2.85	1.09	3.65	2.20
	Elastic Modulus (GPa)	75	45	238	76
Fracture Strain	Mean/std	3.80/0.15	2.42/0.20	1.50*	2.80*

Note: BFRP - Basalt fiber-reinforced polymer, CFRP – Carbon fiber-reinforced polymer, GFRP – Glass fiber-reinforced polymer, * representative values obtained from the literature, where the std is unavailable

It is worth mentioning that the prestress/prestrain of the PT tendons should, on one hand, be sufficiently large to achieve the required "yield" strength and self-centering capability (against friction) of the brace, and on the other hand, be suitably small to provide the necessary deformation capacity. Most of the previous studies[17-22] adopted a prestrain corresponding to around 40% of the ultimate strain, and this prestrain level is also employed in the present study. In other words, the prestrains applied to the MA and MB tendons are 1.5% and 1.0%, respectively, and therefore the mean reserved strains for the two types of tendons are 2.3% and 1.4%, respectively.

Mechanism of brace tendon failure

The tendon failure mechanism of a single-core SCB is straightforward. As shown in Figure 2(a), the PT tendons

in the brace all work in parallel. In the figure, F is the force provided by a group of tendons and D is the deformation of the tendons. The preload applied to each tendon is P, and hence the "yield" resistance of the brace is nP (friction is not considered for the time being), where n is the number of tendons in a tendon set. Keeping the uncertainty of the fracture strain in mind, one PT tendon (PT-1) first fails at a brace deformation of Δ_{s1}, followed by another tendon failing at Δ_{s2}, and so on. The successive occurrence of tendon failure leads to reductions in both the load resistance and post-yield stiffness until all the PT tendons fail and the function of the brace is lost.

The tendon failure mechanism of a dual-core SCB is more complex and perhaps less robust because of the redistribution of the deformation of the different sets of tendons. As shown in Figure 2(b), two sets of PT-tendons (set PT1 and set PT2) work in series, and each set consists of n PT tendons working in parallel. Again, assuming one tendon (PT2-1) first fails at Δ_s (set deformation, which is ideally half the brace deformation), the load resistance of set PT2 decreases while that of set PT1 is unchanged. This unbalanced force leads to redistribution of the deformation because the two sets should always have the same axial force. As a result, the deformation of set PT1 decreases to Δ_s-Δ, and that of set PT2 increases to Δ_s+Δ. Inevitably, some of the remaining tendons in set PT2 are not able to accommodate the increased deformation demand, and therefore fail immediately after the initial tendon failure. This is often a "chain reaction" where all the tendons in set PT2 fail rapidly while those in set PT1 are intact.

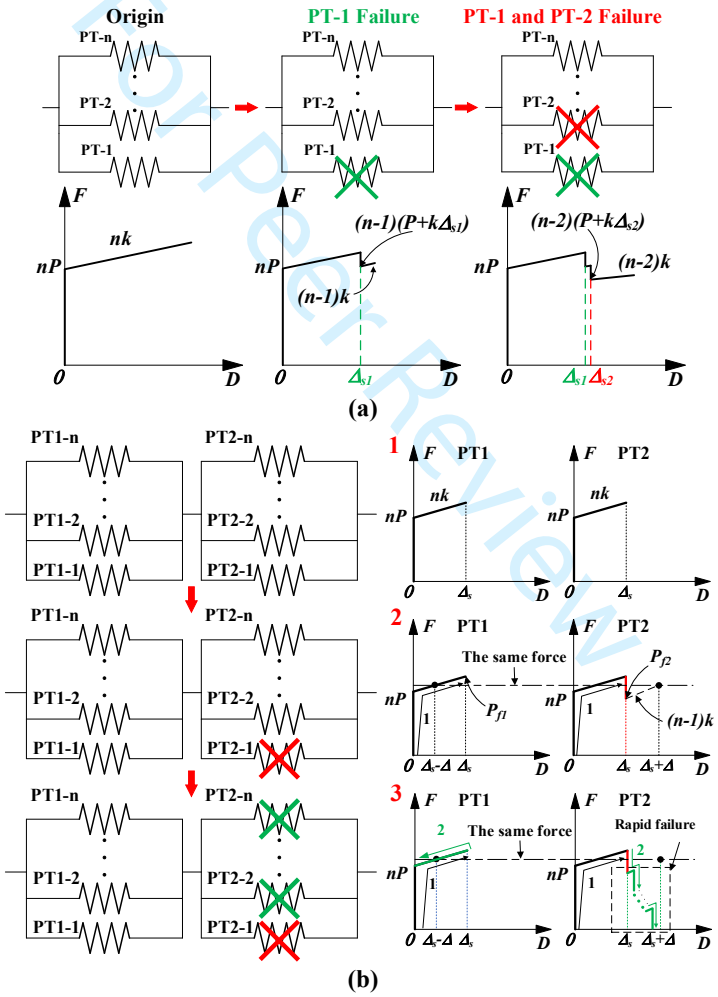

Figure 2 Mechanism of tendon failure: a) single-core SCB, b) dual-core SCB

More specifically, the load resistance of set PT1 (P_{f1}) and set PT2 (P_{f2}) immediately after the initial failure of tendon PT2-1 (i.e., before redistribution of the deformation) can be expressed by:

$$P_{f1} = n(\Delta_s k + P), P_{f2} = (n-1)(\Delta_s k + P) \tag{1.2}$$

where k is the axial (elastic) stiffness of each tendon. There are two possibilities after the initial tendon failure. The first possible scenario is that the load resistance of set PT2 decreases below nP, which indicates that practically the entire deformation demand of the brace has to be provided by set PT2. This scenario would cause immediate fracture of all the PT tendons in set PT2. For the second scenario, if the decreased load resistance of set PT2 is still larger than nP, then the change of the deformation Δ can be expressed by the following equations:

$$P_{f2} + (n-1)k\Delta = P_{f1} - nk\Delta \tag{1.3}$$

$$\Delta = \frac{\Delta_s k + P}{(2n-1)k} \tag{1.4}$$

The relative change of the deformation $(\Delta_s+\Delta)/\Delta_s$ is therefore given by:

$$\frac{\Delta_s + \Delta}{\Delta_s} = \frac{2nk\Delta_s + P}{(2n-1)k\Delta_s} \tag{1.5}$$

Assuming the following typical values for MA tendons: P/A=1125MPa , kL/A=75000MPa , Δ_s/L=0.023 (where L and A are the length and cross-sectional area of each tendon, respectively), and n=5, then $(\Delta_s+\Delta)/\Delta_s$ is 1.184. In other words, all the remaining tendons in set PT2 have to provide at least $0.184\Delta_s$ further deformation without fracture if one wants to stop the "chain reaction". This is highly unlikely given the quality control of the tendon material. Therefore, it can be concluded that in a practical dual-core SCB, once one PT tendon experiences fracture, the remaining tendons in this set are likely to fail immediately afterwards.

PROTOTYPE BUILDINGS

Design of prototype buildings

Following the discussions of the fundamental behavior and failure mechanism of SCBs, this section proceeds with the design and modelling of the prototype buildings incorporating these braces. A series of 9-story steel frames employing different SCBs were designed according to ASCE 7-16[47]. These structures are located on a stiff soil site (Site Class D) in Los Angeles, with the following design response spectral values assigned to the site: S_{DS} = $2/3S_{MS}$ = 1.376g and S_{D1} = $2/3S_{M1}$ = 0.707g. While the braced frames on the perimeter of the building in both directions serve as the lateral load resisting system, this study only focuses on a 2D frame that represents half of the structure in the north-south (NS) direction, as illustrated in Figure 3. Rigid beam-to-column connections are employed for the braced frame, so both the boundary frame and the braces contribute to the lateral load resistance. In other words, a certain level of redundancy is maintained for the considered self-centering structural systems. Modal response spectrum analysis was first conducted to estimate the required base shear and member sizes, where the response modification coefficient (R) and the deflection amplification factor (C_d) were preliminarily taken as 8.0 and 5.0, respectively. Subsequently, nonlinear response history procedure conforming to the ASCE 7-16 requirement was conducted to doublecheck and refine the design where necessary. The allowable mean inter-story drift is 2.0% under the design-based earthquake (DBE).

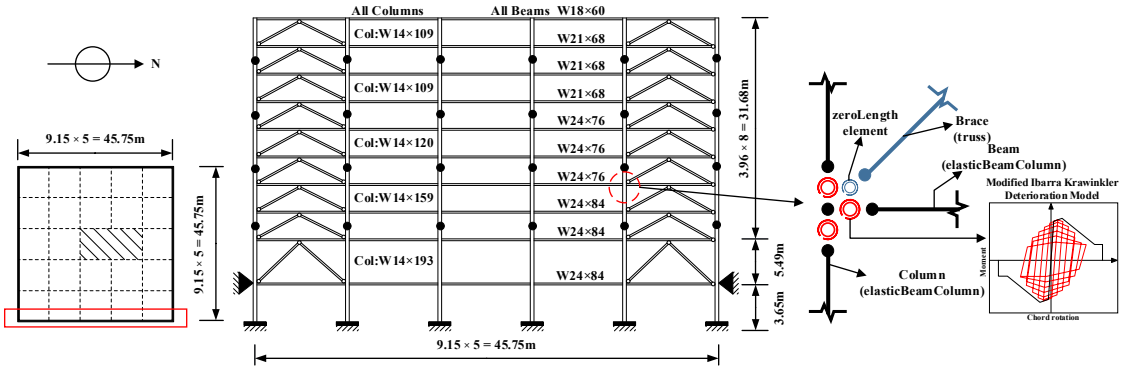

Figure 3 Information of prototype buildings with SCBs

Employing the above procedures, three different self-centering braced frames were carefully designed, namely, 1) frame with single-core SCBs using MA tendons (MASCF), 2) frame with single-core SCBs using MB tendons (MBSCF), and 3) frame with dual-core SCBs using MA tendons (MASCF-D). The effective length of the tendons is 0.85 of the entire brace length, and the prestrain is 40% of the ultimate strain, making sure that no tendon failure happens at the 2.0% inter-story drift limit under the DBE. The number of tendons and the frictional force are tuned such that the braces exhibit an energy dissipation factor β (as illustrated in Figure 1) of approximately 0.95. The detailed design parameters of the SCBs at different floors is summarized in Table 2. It should be noted that K_2 is the post-yield stiffness of each brace which can be calculated according to the material properties and arrangement of the tendons, whereas K_1 is the initial brace stiffness which is more difficult to predict because the value is subjected to large uncertainties related to manufacturing, fabrication, and machining tolerance[17-19,48]. Huang et al.[49] concluded that the initial stiffness of self-centering members is difficult to predict using theoretical equations because of these uncertainties.

In the present study, the value of K_1 is estimated through a comprehensive survey of the existing experimental programs on SCBs with similar configurations, as summarized in Table 3. It is of interest to find that although significant inconsistency exists in the initial stiffness, the initial deformation seems to fall in a relatively narrow range between 1.0 mm and 2.3 mm. Given that the design of the SCBs in these studies is in general similar to that considered in this study, an average initial deformation of 1.8 mm is consistently employed, based on which the initial stiffness (= activation force/initial deformation) can be estimated in Table 2.

Modelling of prototype buildings

Basic centerline models are established and analyzed in the nonlinear dynamic analysis program OpenSees[50]. The boundary frame members are simulated via 'elasticBeamColumn' elements together with 'zeroLength' elements employing Modified Ibarra Krawinkler deterioration model, as shown in Figure 3. The seismic weight is assigned to the 2D frame as well as the adjacent leaning columns to appropriately consider the P-Δ effect. A Rayleigh damping with 5% damping ratio for the first and third modes of vibration is adopted.

The tendon fracture behavior of the brace is fully considered in the model. The self-centering system and friction-based energy dissipation system are modelled independently, as schematically illustrated in Figure 4. The PT tendons are simulated via truss elements with the 'MultiLinearElastic' (MLE) material model. These elements are placed either in parallel or in series, depending on the considered brace configuration (e.g., single- or dual-core SCB). The friction is simulated via 'MultiLinear' (ML) materials, and it is assumed that failure never occurs in the friction device. The truss elements are additionally endowed with a 'MinMax' material model which allows the consideration of tendon fracture. Once the predefined strain is exceeded in the 'MinMax' material, the stiffness and strength immediately decrease to zero. The fracture strains of the different tendons are determined via a random value generator using Monte Carlo methods, considering a normal distribution as previously discussed. In other words, a model considering randomly distributed fracture strain of the tendons is built first, but this particular model is consistently used in the later analysis. The randomly generated probability densities of the fracture strain for the three different frames are shown in Figure 5. It is worth mentioning that according to additional analysis conducted by the authors, different random fracture strain distributions in fact had no significant influence on the structural performance including the residual deformation.

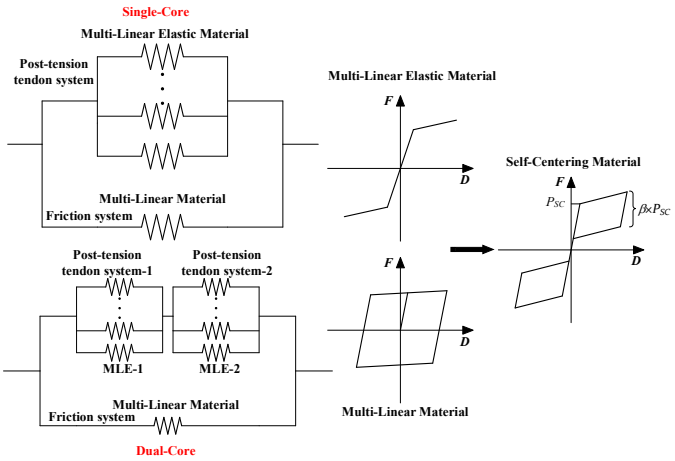

Figure 4 Schematic illustration of SCB model

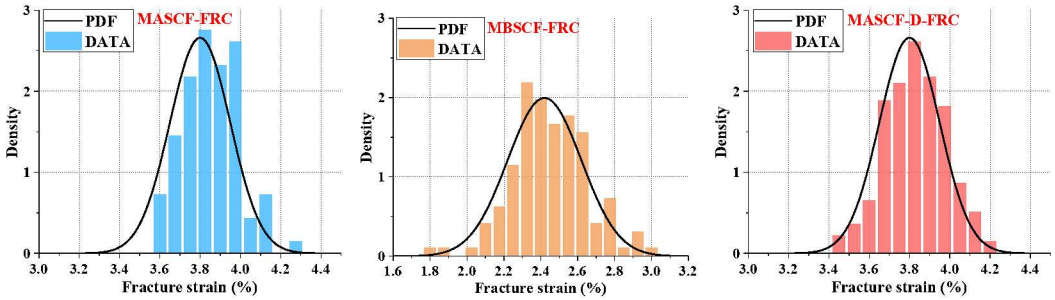

Figure 5 Probability density of fracture strain for different structures

Table 2 Basic design information of SCBs in prototype buildings

Story	MASCF						MBSCF					
	N_{PT}	$P_{PT\text{-}SUM}$	P_{FR}	P_{ACT}	K_1	K_2	N_{PT}	$P_{PT\text{-}SUM}$	P_{FR}	P_{ACT}	K_1	K_2
1	5	636.17	575.58	1211.76	673.20	6.98	7	633.93	573.55	1207.48	670.82	10.43
2	4	508.94	460.47	969.41	538.56	6.60	5	452.80	409.68	862.49	479.16	8.80
3	3	381.70	345.35	727.05	403.92	4.95	4	362.24	327.74	689.99	383.33	7.04
4	3	381.70	345.35	727.05	403.92	4.95	4	362.24	327.74	689.99	383.33	7.04
5	2	254.47	230.23	484.70	269.28	3.30	3	271.68	245.81	517.49	287.50	5.28
6	2	254.47	230.23	484.70	269.28	3.30	3	271.68	245.81	517.49	287.50	5.28
7	2	254.47	230.23	484.70	269.28	3.30	3	271.68	245.81	517.49	287.50	5.28
8	1	127.23	115.12	242.35	134.64	1.65	2	181.12	163.87	344.99	191.66	3.52
9	1	127.23	115.12	242.35	134.64	1.65	1	90.56	81.94	172.50	95.83	1.76

Note: N_{PT} - Number of post-tension tendons, $P_{PT\text{-}SUM}$ – Sum of the post-tension (kN), P_{FR} – Force of the friction system (kN), P_{ACT} – Activation Force (kN), K_1 – Initial stiffness of SCB (kN/mm), K_2 - Post-yield stiffness of SCB (kN/mm)

Table 3 Collection of information on initial stiffness of SCBs

Brace Type	Predicted/Measured	Initial Deformation*
Single-core SCB[17]	/	2.34mm
Single-core SCB[18]	2073/750 kN/mm	2.27mm
Dual-core SCB[19]	1496/230 kN/mm	1.70mm
Dual-core SCB[21]	1200/980 kN/mm	0.92mm
Dual-core SC-BRB[22]	596/585 kN/mm	1.1mm
SC-BRB[23]	/	1.83mm
SC-BRB[24]	/	1.98mm

*: Approximate data

Figure 6 shows the typical axial force-deformation response of individual single- and dual-core SCBs taking account of tendon fracture (where MA tendons are adopted). The two braces are selected from those at the 2nd story of the corresponding prototype buildings. It is confirmed that the single-core SCB fails successively after the initial tendon failure, whereas the failure process is more abrupt for the dual-core SCB. As previously explained, the abrupt failure is due to the rapid redistribution of the deformation of the two sets of tendons in series. For both braces, only the friction device works after the failure of the tendons, and hence the initial flag-shaped hysteretic curve degrades into a rectangular shape.

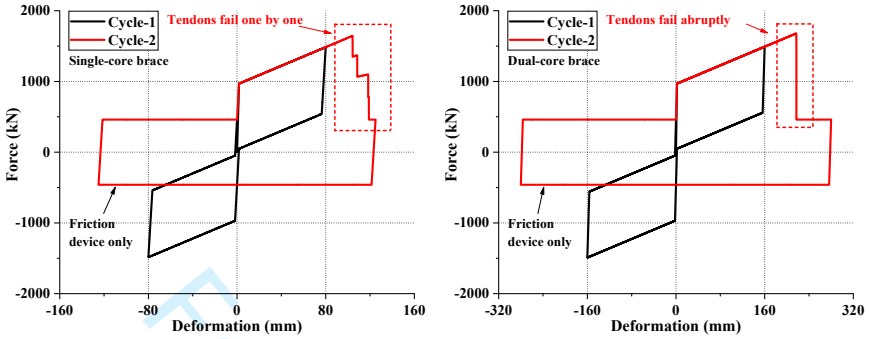

Figure 6 Typical tendon fracture behavior of individual SCBs

Figure 7 further shows the static pushover curves of the three prototype frames. In the following discussions, models MASCF, MBSCF and MASCF-D represent *idealized* frames without considering the tendon failure, and models MASCF-FRC, MBSCF-FRC and MASCF-D-FRC are more *realistic* frames considering the tendon failure behavior. It can be seen that the three frames have similar initial stiffness but vary in the post-yield response. This is expected because the number and arrangement of the tendons differ in the frames. Once tendon fracture first happens, weak story mechanism is often triggered on that particular floor (not reflected in this figure), and as a result, the pushover curves follow a zigzag descending trend until the affected story loses the lateral load resistance. It is clearly seen that MASCF-D-FRC experiences postponed tendon failure because of the dual-core configuration of the SCBs.

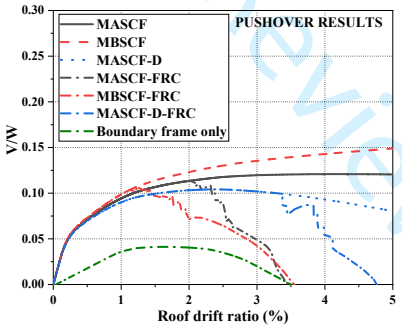

Figure 7 Static pushover curves of prototype buildings (V = base shear, W = seismic weight)

NONLINEAR TIME-HISTORY ANALYSIS

Selected ground motions

The three frames are subjected to 20 pulse-like near-fault (NF) and 20 far-field (FF) ground motions at the maximum considered earthquake (MCE) level. The 20 NF ground motions were selected from the PEER NGA-West database based on the MCE response and the criteria proposed by Baker[51]. The Baker's criteria include three conditions, which are related to the energy of the pulse, the time when the pulse arrives, and the magnitude of the PGV (peak ground velocity). Satisfying the three conditions indicates that the ground motions exhibit typical NF pulsing characteristics. The 20 NF ground motions are unscaled[52] which match the MCE design spectrum, as shown in Figure 8(a). In particular, the mean spectrum is no less than the design response spectrum for periods ranging from $0.2T_1$ to $2.0T_1$, and therefore the ASCE 7-16 requirements are satisfied. On the other hand, another 20 FF ground motions were randomly selected from the far-field ground motion set provided in FEMA P695[53]. This ground motion set was scaled per the method provided by the PEER NGA-West database to represent the

MCE response spectrum, as shown in Figure 8(b). The details of the selected 20 NF and 20 FF ground motions can be found elsewhere[54]. It is worth mentioning that the 40 ground motions are generally sufficient to cover the record-to-record (RTR) variability of ground motions[39], and in particular, the dispersion of residual deformation response, which is sensitive to the ground motion characteristics, can be well captured.

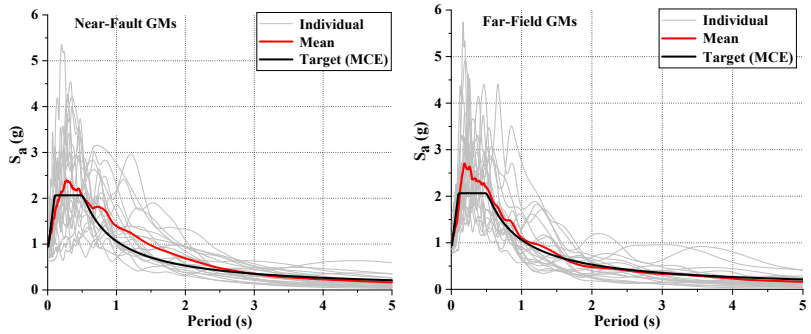

Figure 8 Elastic response spectra of the selected ground motions: a) NF records, b) FF records

Overall response

To facilitate discussion, two collapse limit states are defined in the present study[38,55]: 1) the structure is deemed to be "at a high risk of collapse" if the peak inter-story drift ratio (PIDR) exceeds 5%, and 2) the structure is deemed to have collapsed when the PIDR exceeds 10%. Figure 9 summarizes the number of ground motions causing collapse (or high risk of collapse) of the considered prototype buildings under the MCE. Clearly, excluding the tendon failure behavior evidently underestimates the risk of collapse under both the NF and FF earthquakes. For example, model MBSCF-FRC is at a high risk of collapse under 9 (out of 20) NF ground motions, among which 4 ground motions cause PIDR > 10% (collapse) of the building. Contrarily, the number of ground motions causing collapse of the building is zero if tendon failure is not considered. The risk of collapse is decreased when the MA material is used or dual-core SCBs are employed. Another finding is that the NF earthquakes cause a much higher risk of collapse than the FF earthquakes. This is due to the forward-directivity pulsing effect and hence higher PIDR demands[39].

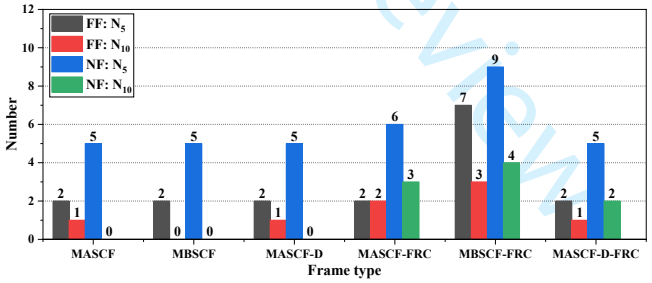

Figure 9 Number of ground motions leading to possible collapse under the MCE (N_5: number of cases with PIDR > 5%; N_{10}: number of cases with PIDR > 10%)

Figure 10(a) shows the mean height-wise PIDR responses of the considered prototype buildings. For fair comparison, any ground motion which may cause collapse (PIDR > 10%) of any one of the models are not included when calculating the mean responses. Counterintuitively, taking tendon fracture into account does not always lead to increased mean PIDRs under the MCE. There could be several reasons for this. Firstly, quite a number of MCE-level ground motions do not cause tendon fracture of the SCB, which neutralizes the difference in the mean structural response, especially when the extremes cases (PIDR > 10%) are excluded. Secondly, the structures are designed as dual systems where the boundary frame and the friction devices continue contributing to the lateral load resistance and therefore the effect of tendon fracture may not be that critical. Thirdly, the initial occurrence of tendon fracture at a certain floor can sometimes alleviate the PIDR at other floors; this can be confirmed in the case study presented later. The results also show that the frame with dual-core SCBs does not always exhibit the smallest PIDR response, and this may be related to its small post-yield stiffness, as can be seen from the pushover curves. Being in line with Figure 9, the NF earthquakes cause increased PIDR responses than the FF earthquakes.

Figure 10(b) shows the mean height-wise residual inter-story drift ratio (RIDR) of the buildings. The occurrence of tendon fracture significantly compromises the self-centering capability, especially for model MBSCF-FRC which has the smallest deformation capacity of the SCBs. The difference in the tendency displayed by the PIDR and RIDR responses is because the friction device alone has no self-centering function but does provide energy dissipation, so the PIDR is not critically affected but the structures lose the control of the RIDR. Again, the NF earthquakes cause increased RIDR because of the pulsing effect. For model MBSCF-FRC, the mean maximum RIDR is close to 1.0%. According to the FEMA P-58 definition[56], the RIDR-related damage state approaches class DS4, i.e., the residual deformation may be too large that the structure is in danger of collapse from aftershocks. Increasing the deformation capacity of the SCBs can mitigate the RIDR. The mean maximum RIDR is 0.5% or less for models MASCF-FRC and MASCF-D-FRC, i.e., structural repairs are necessary, but degradation in structural stability is limited[56]. The detailed damage states defined in FEMA P-58 will be elaborated later.

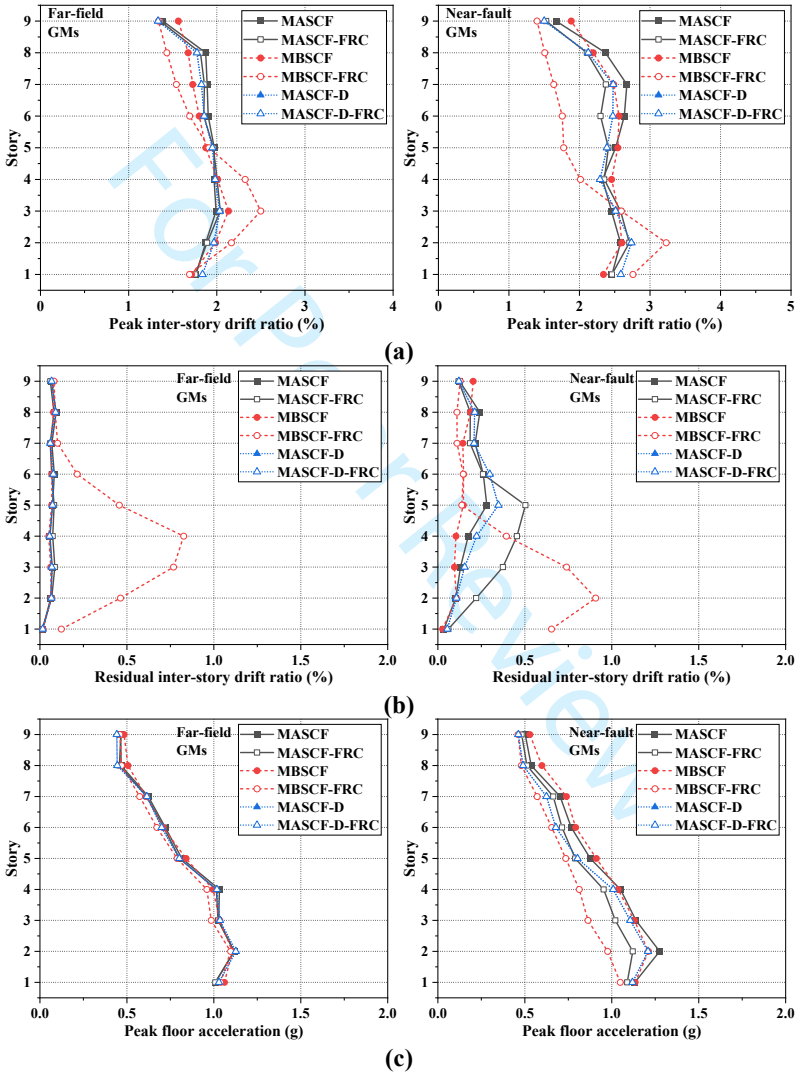

Figure 10 Mean seismic responses of prototype structures under the MCE: a) peak inter-storey drift ratio (PIDR), b) residual inter-storey drift ratio (RIDR), c) peak floor acceleration (PFA)

Figure 10(c) shows the distributions of the mean peak floor acceleration (PFA) of the prototype buildings. Tendon fracture seems to have a limited influence on the PFA responses; in other words, the PFA-induced non-structural damage is not increased because of the tendon fracture. A possible explanation is that the inconsistent inter-story shear forces of two adjacent floors are not increased when the tendons quit working, noting that the difference in the story shear directly attributes to the PFA[57]. Another possible reason is that after the fracture of the tendons, a full hysteretic response is exhibited (i.e., the friction behavior), and hence less "transition points" occur in the hysteretic loop compared with the flag-shaped hysteresis. Previous studies[57] showed that frequent transitions in

the hysteresis are more likely to produce short duration, high amplitude PFA pulses.

Case study

Following the discussion of the overall structural responses, this section takes an in-depth look at some representative individual cases to foster a better understanding of the behavior of the structures after tendon fracture. Figures 11(a) and 11(b) show two contradictory cases where the occurrence of tendon fracture increases and decreases the PIDR, respectively. As shown in Figure 11(a), initial tendon fracture happens in model MASCF-FRC at 1st-3rd story at 11~12 seconds when subjected to ground motion NF-1. The induced inter-story drift is not recovered, and weak story mechanism is then formed with excessive deformation concentrated at the soft stories, resulting in final collapse of the structure. On the other hand, under ground motion NF-13, model MBSCF-FRC first experiences tendon fracture at the 1st and 2nd story at around 3.5 seconds, and 3rd story at around 6.3 seconds. The inter-story drifts at these stories are developed but without evolving into weak stories, perhaps attributed to a favorable ground excitation that helps restore the drifts at that moment. Nevertheless, the tendon fracture at the lower stories alleviates the PIDR of the 7th story, noting that this story is supposed to exhibit the largest PIDR for the idealized structure (model MBSCF) at around 7.4 seconds. This case implies that tendon fracture at a certain story can also affect the inter-story drifts at other floors, and whether weak story mechanism is formed depends on the dynamic characteristics of both the structure and the ground motion, which is not easily predictable.

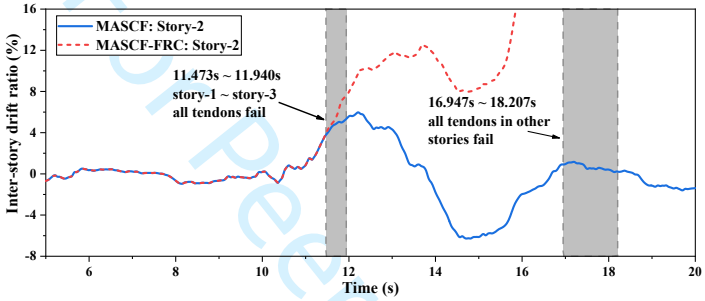

(a)

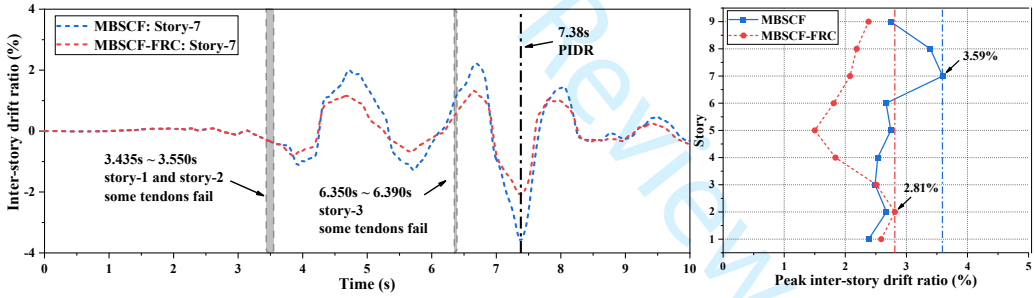

(b)

Figure 11 Representative inter-story drift ratio time-histories: a) MASCF series under NF-1, b) MBSCF series under NF-13

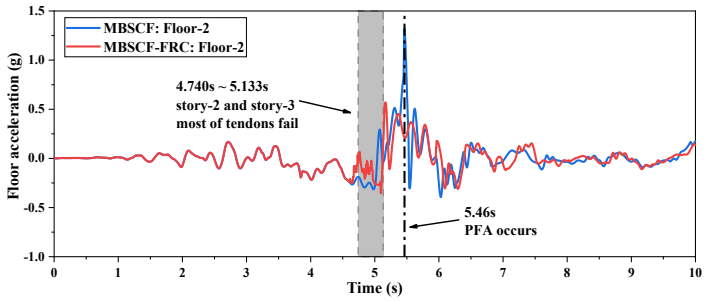

(a)

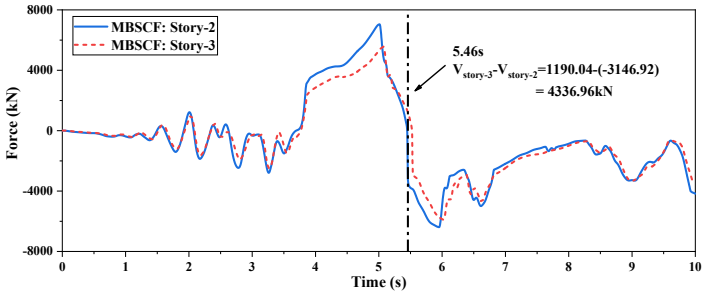

(b)

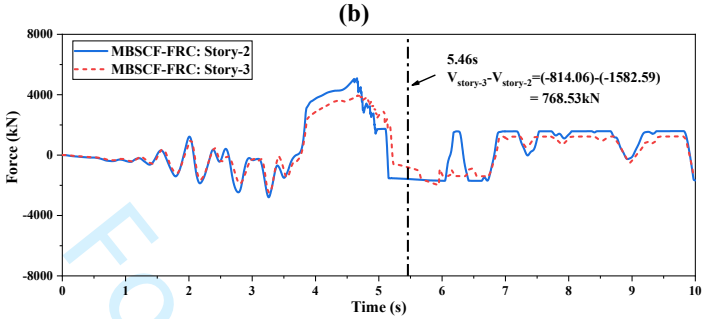

(c)

Figure 12 Influence of tendon fracture on PFA: a) floor acceleration time-histories, b) brace force histories of model MBSCF, c) brace force histories of model MBSCF-FRC under NF-11

Ground motion NF-11 is used to demonstrate the influence of tendon fracture on the PFA response. The floor acceleration time-histories of models MBSCF and MBSCF-FRC under this ground motion are presented in Figure 12(a), where a large-amplitude PFA pulse is observed at floor level 2 of the idealized model (MBSCF) at around 5.5 seconds. No such behavior is observed when tendon fracture is considered in model MBSCF-FRC. As aforementioned, a large PFA is attributed to inconsistent inter-story shear forces of the two adjacent floors, where one story has the shear force lagging that of the neighboring story during the ground excitation. Figure 12(b) confirms this lagging effect by showing the sum of the brace force at the 2nd and 3rd stories. A large transient difference in the brace force (4337 kN) occurs at 5.5 seconds, which is directly responsible for the large PFA pulse. On the other hand, the difference in the brace force decreases to 769 kN after the occurrence of tendon fracture, as shown in Figure 12(c), and hence the PFA is decreased. It should be noted that opposite tendencies may be observed for the same structures under other ground motions. Statistically speaking, there seems to be no obvious correlation between tendon fracture and PFA response.

FRAGILITY ANALYSIS AND RISK ASSESSMENT

Assumptions and definitions

Following the nonlinear time-history analysis of the prototype buildings under the MCE, the performance of these frames is probabilistically assessed through collapse and residual deformation fragility analysis. Incremental dynamic analysis (IDA)[58] is carried out on the structural models subjected to the aforementioned 40 records. The uncertainty of tendon fracture strain is considered in the structural models; other structural-related uncertainties (e.g., material property and member size) are not considered. The maximum PIDR among all the floors (θ_{pmax}) and the maximum RIDR among all the floors (θ_{rmax}) are considered as the Damage Measures (DMs). The Intensity Measure (IM) is the 5% damped spectral acceleration at the fundamental period T_1, i.e., $S_a(T_1)$. Apart from the previous definition of collapse (PIDR > 10%) for the nonlinear time-history analysis, collapse for the fragility analysis is additionally defined by the following two more events[55,58]: 1) the IDA curve is nearly "flat" when the slope becomes less than 0.2 times the initial slope, and 2) instability (non-convergence) occurs during the analysis. The three collapse criteria, i.e., θ_{pmax} > 10%, flat IDA curve, and instability of analysis, are often called DM, IM, and instability collapse criteria, respectively. If more than one collapse criterion are identified, the smaller $S_a(T_1)$ is adopted. The detailed process for defining collapse is illustrated in Figure 13. The increment of $S_a(T_1)$ is 0.05~0.1 g until the defined "collapse" occurs for each frame.

For the residual deformation response, four DMs, corresponding to four θ_{rmax} thresholds, are defined in FEMA P-58. The strictest class, DS1, requires that θ_{rmax} is less than 0.2% such that "no structural realignment is necessary for structural stability, but the building may require adjustment and repairs to non-structural and mechanical

components". A relaxed class of DS2 requires that the θ_{rmax} is no more than 0.5% in order to make economically feasible realignment of structural frame and related structural repairs, with limited degradation in structural stability. DS2 is generally consistent with the survey made by McCormick et al.[2] who concluded that a residual drift ratio exceeding 0.5% leads to prohibitively high repair cost for the structure. Class DS3 with a θ_{rmax} limit of 1.0% indicates that major structural realignment is needed to restore lateral stability, although the work could be economically and practically infeasible. Class DS4 with a θ_{rmax} limit of 2.0% indicates that the structure is in danger of collapse during aftershocks.

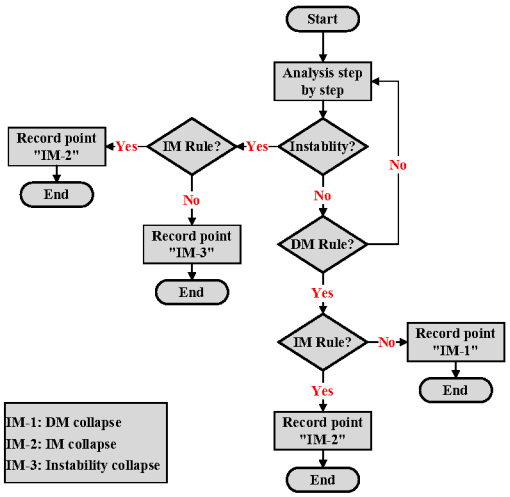

Figure 13 Process for the definition of collapse for IDA analysis

Collapse fragility analysis results

The individual and the 16%, 50%, and 84% percentile IDA curves associated with θ_{pmax} of the considered frames are shown in Figure 14, reminding that the models ending with "FRC" are those considering tendon fracture. For clearer interpretation in the following discussions, the seismic intensity is represented by $S_a(T_1)$ normalized by $S_{aMCE}(T_1)$, where $S_{aMCE}(T_1)$ is the 5% damped spectral acceleration at the fundamental period T_1 of each frame under the MCE. It can be seen that the three idealized frames exhibit similar tendencies, and the IDA curves are generally stable. This is because of the ignorance of the degradation effect caused by tendon fracture. When tendon fracture is considered, the IDA curves experience earlier flat stage, especially for model MBSCF-FRC which has the smallest tendon fracture strain.

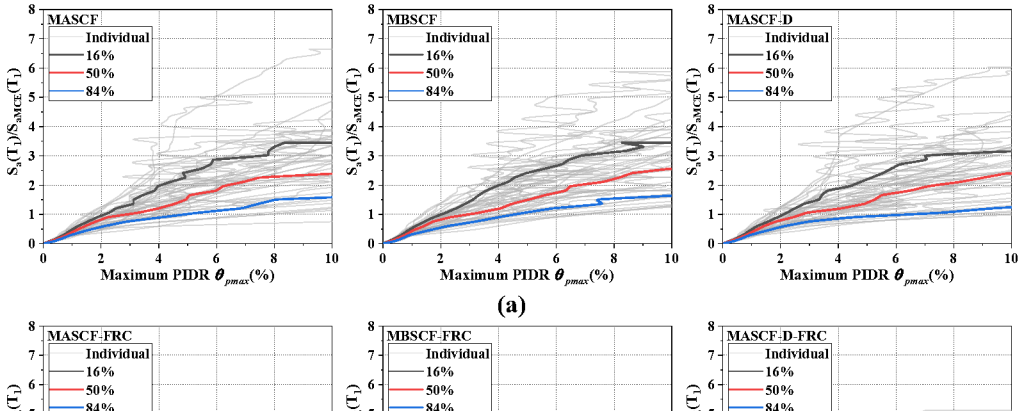

(a)

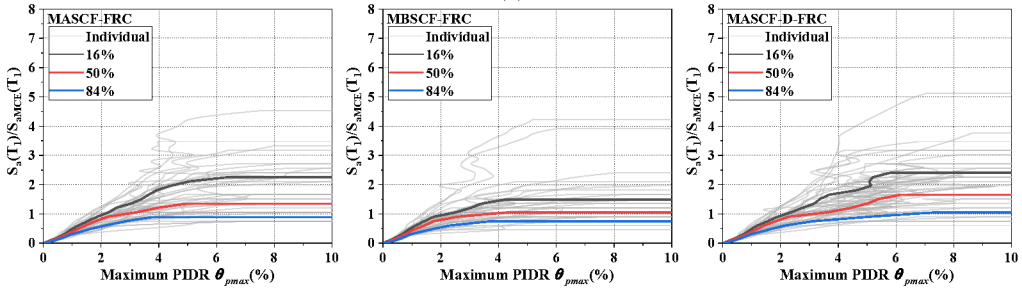

(b)

Figure 14 IDA curves: a) idealized frames, b) frames considering tendon fracture

The probability of collapse at a certain IM is the number of cases that cause collapse out of the total number of analysis. The collapse fragility curves with increasing normalized IMs can be constructed based on the IDA results, fitted by a lognormal cumulative distribution function (CDF) as expressed by:

$$CDF(x) = \int_0^X \frac{1}{\sqrt{2\pi}\beta x} \exp\left[\frac{(\log x - \log CMR)^2}{2\beta^2}\right] dx \tag{1.6}$$

$$CMR = \frac{S_{a,50\%}(T_1)}{S_{aMCE}(T_1)} \tag{1.7}$$

where x is the random variable, i.e., $S_a(T_1)/S_{aMCE}(T_1)$ in the context of this study. CMR (collapse margin ratio) is the $S_a(T_1)/S_{aMCE}(T_1)$ value corresponding to 50% probability of collapse, where a larger CMR indicates a better collapse resistance. The collapse fragility curves of the idealized model and the model considering tendon fracture are compared in Figure 15(a) through 15(c), and the CMR and the associated standard deviation (β) are summarized in Table 4.

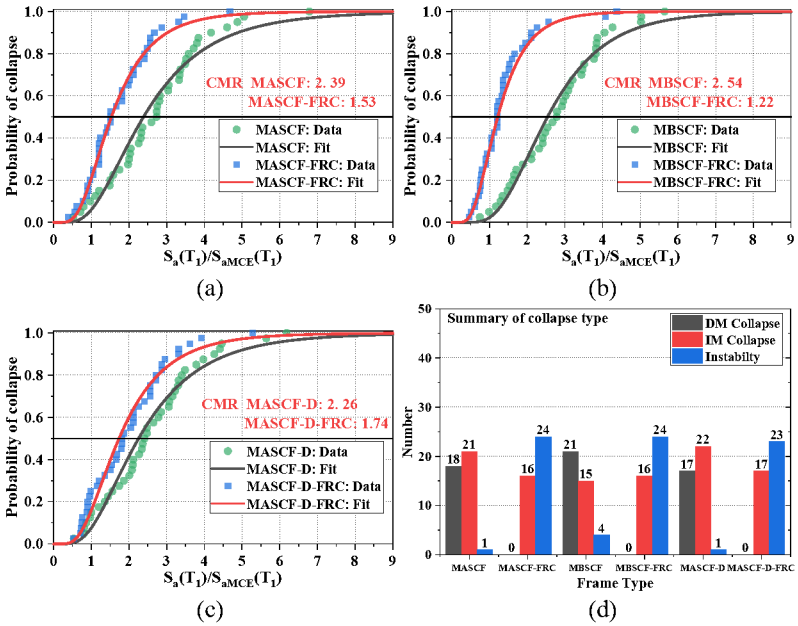

Figure 15 Collapse fragility analysis results: a) MASCF series models, b) MBSCF series models, c) MASCF-D series models, d) summary of types of collapse

Table 4 Summary of collapse and residual deformation fragility analysis results

Frame type	*CMR*	*DMR* 0.2%	0.5%	1.0%	2.0%
MASCF	2.39(0.56)	1.69(0.70)	2.06(0.61)	2.25(0.58)	2.31(0.59)
MBSCF	2.54(0.48)	1.77(0.66)	2.31(0.52)	2.42(0.50)	2.43(0.50)
MASCF-D	2.26(0.57)	1.51(0.68)	1.89(0.63)	2.05(0.59)	2.15(0.60)
MASCF-FRC	1.53(0.53)	0.97(0.43)	1.25(0.53)	1.30(0.55)	1.34(0.56)
MBSCF-FRC	1.22(0.50)	0.85(0.43)	0.97(0.50)	1.03(0.52)	1.05(0.53)
MASCF-D-FRC	1.74(0.55)	1.29(0.60)	1.44(0.58)	1.50(0.58)	1.56(0.58)

The fragility curves of the three idealized frames are similar. The minor difference is attributed to the different post-yield responses (stiffness) of the three frames. When tendon fracture is considered, the fragility curves move leftwards, indicating that the probability of collapse increases at the same level of IM. For instance, the probability of collapse for model MBSCF is less than 3% under the MCE, i.e., $S_a(T_1)/S_{aMCE}(T_1) = 1.0$, whereas that probability increases tremendously to around 34% for the same structure under the same level of earthquake, with tendon

fracture considered. This observation generally echoes the nonlinear time-history results which showed that quite a number of MCE-level ground motions caused collapse (or high risk of collapse) of the structure. Increasing the fracture strain or adopting a dual-core SCB configuration tend to decrease the probability of collapse. From a median probability point of view, the *CMR* values of models MASCF, MBSCF, and MASCF-D are decreased by 36%, 52%, and 23%, respectively, when tendon fracture is considered. The above results reaffirm that the risk of collapse is closely related to the available deformability of the SCBs, especially for the structures with single-core SCBs. The collapse fragility is less sensitive to the consideration of tendon fracture when dual-core SCBs are employed.

The influence of tendon fracture on the collapse behavior can be further revealed in Figure 15(d) which summaries the number and type of "collapse" for the different structures under the 40 ground motions with increasing IM. The collapse of the idealized frames is mainly governed by the DM and IM criteria, where the latter could be related to the deterioration of the connections. On the other hand, the collapse of the frames considering tendon fracture happens mostly because of the instability and IM criteria, which indicates that the degradation of strength and stiffness trigger early collapse prior to reaching the 10% θ_{pmax} limit.

Residual deformation fragility analysis results

The RIDR fragility curves that provide the probability of exceedance of θ_{rmax} = 0.2%, 0.5%, 1.0% and 2.0% are shown in Figure 16. The values of $S_a(T_1)/S_{aMCE}(T_1)$ with 50% probability of exceedance of each θ_{rmax} are summarized in Table 4 together with the associated standard dispersion β. It should be noted that for the cases when the collapse criteria are exceeded (collapse has occurred), θ_{rmax} is then taken as a large value (e.g., 10%). Clearly, the fragility curves consistently move leftwards when tendon fracture is considered, indicating increased probability of exceedance of the considered θ_{rmax} limits. Taking model MASCF under the MCE as an example, the probability of exceedance of 0.5% limit increases from 12% to 33% when tendon fracture is considered. In other words, there is a 33% probability that the structure needs to receive major structural realignment when seeing an MCE-level earthquake, and the work, according to McCormick et al.[2], may be economically and technically infeasible, leaving demolition is the only option. For model MBSCF, the probability of exceedance of 0.5% θ_{rmax} limit increases more tremendously from 5% to 52% when tendon fracture is considered, which is because of the reduced deformability of the SCBs. The probability of exceedance is less significantly changed for model MASCF-D when considering tendon fracture, especially when $S_a(T_1)/S_{aMCE}(T_1)$ is small. This is attributed to the enhanced elongation of the dual-core SCBs. As the median $S_a(T_1)/S_{aMCE}(T_1)$ given in Table 4 is similar to the concept of *CMR*, these values are called damage margin ratio (*DMR*), where a larger *DMR* means enhanced RIDR control capability.

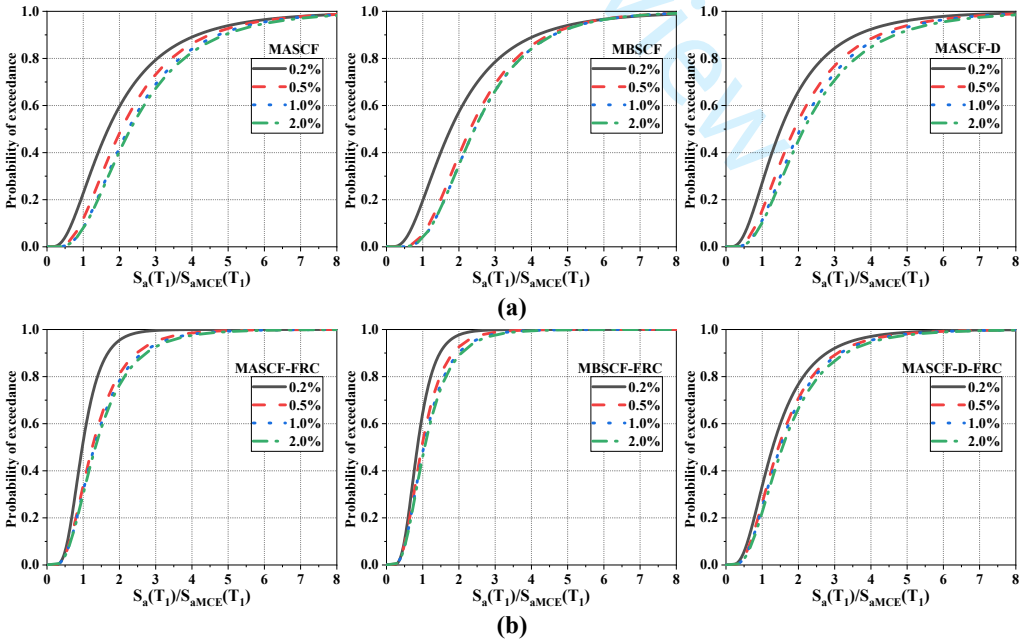

Figure 16 RIDR fragility curves: a) idealized frames, b) frames considering tendon fracture

Risk assessment

Further to the fragility analysis, the collapse and self-centering performances of the structures can be more clearly presented by the mean annual frequency of collapse, λ_C, and the mean annual frequency of exceeding a specified limit of maximum RIDR, λ_{MR}, respectively, given the site of the structure. The specific site determines the annual frequency of exceedance of the spectral acceleration λ_{Sa}. Given that the considered frames are located on a stiff soil site (Site Class D) in Los Angeles, the hazard data of λ_{Sa} can be obtained from the U.S. Geological Survey (USGS) website[59] using linear interpolation, as shown in Figure 17. Then λ_C and λ_{MR} are obtained by the integrations of the collapse and RIDR fragility curves over the λ_{Sa} curve, respectively, as expressed by:

$$\lambda_C = \int_0^\infty P\left(C|S_a\right)\left|\frac{d\lambda_{S_a}\left(S_a\right)}{dS_a}\right|dS_a \tag{1.8}$$

$$\lambda_{MR} = \int_0^\infty P\left(MR|S_a\right)\left|\frac{d\lambda_{S_a}\left(S_a\right)}{dS_a}\right|dS_a \tag{1.9}$$

where $P(C|S_a)$ and $P(MR|S_a)$ are the probabilities of collapse and exceedance of certain θ_{rmax} limit, respectively, given a certain IM, i.e., Sa(T_1). Alternatively, the risk assessment can be conducted over the entire service life of the structure, e.g., n = 50 years. Assuming a Poisson distribution for the occurrence of earthquake with time, the probability of collapse over n years, P_{nC}, and the probability of exceeding a specific θ_{rmax} limit over n years, P_{nMR}, can be converted from λ_C and λ_{MR}, respectively:

$$P_{nC} = 1 - \exp(-\lambda_C n) \tag{1.10}$$

$$P_{nMR} = 1 - \exp(-\lambda_{MR} n) \tag{1.11}$$

The risk assessment results are summarized in Table 5. The three idealized frames have probability of collapse over 50 years of 1.25~2.12%, which seem acceptable; however, when tendon fracture is included in the analysis, the probability of collapse increased evidently from 3.58~6.52%. The risk of collapse for model MBSCF-FRC is more than 5 times that of the idealized model MBSCF. Using MA tendon material decreases the probability of collapse from 6.52% to 4.39%, and a dual-core SCB design can further decrease the probability to 3.58%. For the residual deformation performance, the consideration of tendon fracture consistently increases the probability of exceedance. Taking a θ_{rmax} limit of 0.5% as an example, the probability of exceedance for model MBSCF-FRC reaches 9.71%, which means that there is a 9.71% chance that the structure has to receive major structural realignment over its 50-year service period. The probability of exceedance decreases to 5.46-6.56% when the other two SCB solutions are adopted. Such data could be helpful to engineers, owners, insurers, and other stakeholders during the decision-making process.

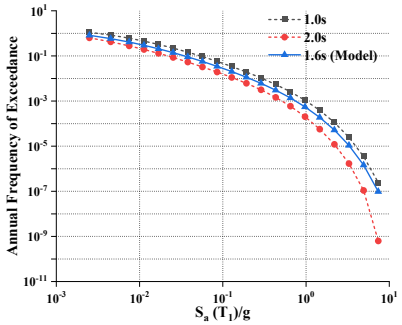

Figure 17 Hazard data of λ_{Sa} obtained from USGS

Table 5 Summary of risk assessment results

Frame	Event	COLLAPSE	Maximum RIDR			
			0.2%	0.5%	1.0%	2.0%
MASCF	λ_C, λ_{MR}	3.70E-04	1.06E-03	5.79E-04	4.44E-04	4.29E-04

MBSCF	P_{50C}, P_{50MR}	1.83%	5.17%	2.85%	2.20%	2.12%
	λ_C, λ_{MR}	2.52E-04	8.96E-04	3.58E-04	3.03E-04	3.03E-04
MASCF-D	P_{50C}, P_{50MR}	1.25%	4.38%	1.78%	1.50%	1.50%
	λ_C, λ_{MR}	4.28E-04	1.25E-03	7.20E-04	5.60E-04	5.19E-04
MASCF-FRC	P_{50C}, P_{50MR}	2.12%	6.07%	3.54%	2.76%	2.56%
	λ_C, λ_{MR}	8.98E-04	1.86E-03	1.36E-03	1.28E-03	1.25E-03
MBSCF-FRC	P_{50C}, P_{50MR}	4.39%	8.89%	6.56%	6.22%	6.04%
	λ_C, λ_{MR}	1.35E-03	2.38E-03	2.04E-03	1.91E-03	1.85E-03
MASCF-D-FRC	P_{50C}, P_{50MR}	6.52%	11.24%	9.71%	9.12%	8.84%
	λ_C, λ_{MR}	7.28E-04	1.44E-03	1.12E-03	1.05E-03	9.72E-04
	P_{50C}, P_{50MR}	3.58%	6.94%	5.46%	5.11%	4.74%

SUMMARY AND CONCLUSIONS

This paper has comprehensively discussed the "seismic robustness" of self-centering braced frames considering the risk of tendon failure. The fundamental mechanism of tendon failure in SCBs was first introduced, followed by the design and analysis of a series of prototype buildings with different tendon materials and brace configurations. The dynamic behavior of the frames was then assessed by a suite of ground motion records, covering both far-field and near-fault ones. The collapse and residual deformation fragilities of the frames were further assessed, and finally the study ended with a risk assessment providing the probability of collapse or exceedance of certain residual deformation over the 50-year service period. The main findings and conclusions are noted as follows.

- The failure mechanism of SCBs was revealed, which suggested that a single-core SCB fails successively after the initial tendon failure, whereas the failure process is more abrupt for dual-core SCBs because of the redistribution of the deformation of the different sets of tendons. In practice, once one PT tendon in a dual-core SCB experiences fracture, the remaining tendons in that set are likely to fail immediately afterwards.
- Tendon fracture does not always lead to increased PIDR responses because there is a mutual effect between the story that first fails and the other critical stories; moreover, whether weak story mechanism is triggered due to tendon fracture depends on the inherent characteristics of both the structure and the ground motion.
- The occurrence of tendon fracture significantly compromises the self-centering capability because the friction device alone has no self-centering function. The increase in RIDR due to tendon fracture is more evident under the NF earthquakes because of the pulsing effect which tends to accumulate the residual deformation.
- There is no obvious statistical correlation between tendon fracture and the PFA, suggesting that the PFA-induced non-structural damage is not necessarily increased because of the tendon fracture. This observation may be associated with the fact that the inconsistent inter-story shear force, which is responsible for the production of the PFA, is insensitive to tendon fracture.
- The probabilities of collapse and exceedance of certain residual drift both increase evidently when tendon fracture is considered, e.g., the *CMR*s of models MASCF, MBSCF, and MASCF-D are decreased by 36%, 52%, and 23%, respectively, and the *DMR*s of the same models are decreased by 39%, 58%, and 24%, respectively, given a 0.5% θ_{rmax} limit. The failure probabilities are closely related to the available deformability of the SCBs, where dual-core SCBs showed less sensitivity to tendon fracture.
- The probability of collapse of the three frames over 50 years of service increases from 1.25~2.12% to 3.58~6.52% when tendon fracture is considered. Considering a θ_{rmax} threshold of 0.5%, the probability of exceedance of the same structures over the same service life increases from 1.78~3.54% to 5.46~9.71%.

Based on the limited data from the present study, it may be safe to ignore tendon fracture for the analysis of the structures with dual-core SCBs under FF earthquakes with a magnitude up to the MCE level, whereas a realistic modelling of the tendon fracture is desired for the case of single-core SCBs. When pulse-like NF effect is of interest or for any analysis beyond the MCE, tendon fracture needs to be considered for both single- and dual-core SCBs. The above preliminary conclusion also depends on the type of analysis and design intention. Finally, it is worth emphasizing that the above conclusions are made based on the behavior of dual systems (i.e., the boundary frame contributes to lateral load resistance), and on the condition that no failure occurs in the friction device.

ACKNOWLEDGEMENTS

The financial supports from the National Natural Science Foundation of China (NSFC) with Grant Nos. 51778456, 52078359 and 51820105013 are gratefully acknowledged. Support for this study was also provided by the Shanghai Rising-Star Program (20QA1409400).

REFERENCES

1. Wood A, Noy I, Parker M. The Canterbury rebuild five years on from the Christchurch earthquake. *Reserve Bank of New Zealand Bulletin.* 2016;79(3):1–16.
2. McCormick, Jason, et al. Permissible residual deformation levels for building structures considering both safety and human elements. *Proceedings of the 14th world conference on earthquake engineering*. Seismological Press Beijing, 2008.
3. Erochko J, Christopoulos C, Tremblay R, Choi H. Residual drift response of SMRFs and BRB frames in steel buildings designed according to ASCE 7-05. *Journal of Structural Engineering*. 2011, 137(5): 589-99.
4. Ricles JM, Sause R, Garlock M, Zhao C. Post-tensioned seismic resistant connections for steel frames. *Journal of Structural Engineering*. 2001; 127(2): 113-121.
5. Ricles JM, Sause R, Peng SW, Lu LW. Experimental evaluation of earthquake resistant post-tensioned steel connections. *Journal of Structural Engineering*. 2002; 128(7): 850-859.
6. Lin YC, Sause R, Ricles JM. Seismic performance of a steel self-centering moment resisting frame: hybrid simulations under design basis earthquake. *Journal of Structural Engineering*. 2013;139(11):1823-1832.
7. Zhang AL, Zhang YX, Li R, Wang ZY. Cyclic behavior of a prefabricated self-centering beam–column connection with a bolted web friction device. *Engineering Structures*. 2016, 111: 185-198.
8. Li Z, He M, Wang K. Hysteretic performance of self-centering glulam beam-to-column connections. *Journal of Structural Engineering*. 2018;144(5):04018031.
9. Kam WY, Pampanin S, Palermo A, Carr AJ. Self-centering structural systems with combination of hysteretic and viscous energy dissipations. *Earthquake engineering & structural dynamics*. 2010, 39(10): 1083-1108.
10. Tzimas AS, Kamaris GS, Karavasilis TL, Galasso C. Collapse risk and residual drift performance of steel buildings using post-tensioned MRFs and viscous dampers in near-fault regions. *Bulletin of Earthquake Engineering*. 2016, 14(6): 1643-1662.
11. Feng W, Fang C, Wang W. Behavior and design of top flange-rotated self-centering steel connections equipped with SMA ring spring dampers. *Journal of Constructional Steel Research.* 2019;159:315-329.
12. Fang C, Wang W, Feng W. Experimental and numerical studies on self-centering beam-to-column connections free from frame expansion. *Engineering Structures.* 2019; 198: 109526.
13. Chou CC, Chen JH. Seismic design and shake table tests of a steel post-tensioned self-centering moment frame with a slab accommodating frame expansion. *Earthquake Engineering & Structural Dynamics.* 2011;40(11):1241-1261.
14. Chou CC, Chen JH. Development of floor slab for steel post-tensioned self-centering moment frames. *Journal of Constructional Steel Research*. 2011;67(10):1621-1635.
15. Garlock MEM, Li J. Steel self-centering moment frames with collector beam floor diaphragms. *Journal of Constructional Steel Research.* 2008;64(5):526-538.
16. Shu Z, Li Z, He M, et al. Seismic design and performance evaluation of self-centering timber moment resisting frames[J]. *Soil Dynamics and Earthquake Engineering.* 2019;119:346-357.
17. Christopoulos C, Tremblay R, Kim HJ, Lacerte M. Self-centering energy dissipative bracing system for the seismic resistance of structures: development and validation. *Journal of Structural Engineering*. 2008;134(1):96-107.
18. Erochko J, Christopoulos C, Tremblay R. Design, testing, and detailed component modeling of a high-capacity self-centering energy-dissipative brace. *Journal of Structural Engineering.* 2015; 141(8): 04014193.
19. Erochko J, Christopoulos C, Tremblay R. Design and testing of an enhanced-elongation telescoping self-centering energy-dissipative brace. *Journal of Structural Engineering.* 2015;141(6):04014163.
20. Chou C C, Chen Y C. Development and seismic performance of steel dual-core self-centering braces. *15th world conference on Earthquake Engineering*, 2012.
21. Chou C C, Chung P T. Development of cross-anchored dual-core self-centering braces for seismic resistance. *Journal of Constructional Steel Research*. 2014;101:19-32.
22. Chou C C, Tsai W J, Chung P T. Development and validation tests of a dual-core self-centering sandwiched buckling-restrained brace (SC-SBRB) for seismic resistance. *Engineering Structures*. 2016;121:30-41.
23. Zhou Z, Xie Q, Lei XC, He XT, Meng SP. Experimental investigation of the hysteretic performance of dual-tube self-centering buckling-restrained braces with composite tendons. J*ournal of Composites for Construction.* 2015;19(6):04015011.
24. Miller DJ, Fahnestock LA, Eatherton MR. Development and experimental validation of a nickel-titanium shape memory alloy self-centering buckling-restrained brace. *Engineering Structures*. 2012; 40:288-298.

25. Qiu C, Zhu S. Shake table test and numerical study of self-centering steel frame with SMA braces. *Earthquake Engineering & Structural Dynamic*. 2017;46(1):117-137.
26. Qiu C, Zhu S. Performance-based seismic design of self-centering steel frames with SMA-based braces. *Engineering Structures*. 2017;130:67-82.
27. Moradi S, Alam M S, Asgarian B. Incremental dynamic analysis of steel frames equipped with NiTi shape memory alloy braces. *The Structural Design of Tall and Special Buildings*. 2014;23(18):1406-1425.
28. Xu X, Zhang Y, Luo Y. Self-centering eccentrically braced frames using shape memory alloy bolts and post-tensioned tendons. *Journal of Constructional Steel Research*. 2016;125:190-204.
29. Abou-Elfath H. Evaluating the ductility characteristics of self-centering buckling-restrained shape memory alloy braces. *Smart Materials and Structures*. 2017;26(5):055020.
30. Massah S R, Dorvar H. Design and analysis of eccentrically braced steel frames with vertical links using shape memory alloys. *Smart materials and structures*. 2014;23(11):115015.
31. Yang CSW, Desroches R, Leon RT. Design and analysis of braced frames with shape memory alloy and energy-absorbing hybrid devices. *Engineering Structures*. 2010;32(2):498-507.
32. Vafaei D, Eskandari R. Seismic performance of steel mega braced frames equipped with shape-memory alloy braces under near-fault earthquakes. *Structural Design of Tall and Special Buildings*. 2016;25:3-21.
33. Wang W, Fang C, Zhang A, et al. Manufacturing and performance of a novel self-centering damper with shape memory alloy ring springs for seismic resilience. *Structural Control and Health Monitoring*. 2019; 26(5): e2337.
34. Chen J, Fang C, Wang W, Liu Y. Variable-friction self-centering energy-dissipation braces (VF-SCEDBs) with NiTi SMA cables for seismic resilience. *Journal of Constructional Steel Research.* 2020, Under Review.
35. Wang W, Fang C, Zhao Y, et al. Self-centering friction spring dampers for seismic resilience. *Earthquake Engineering & Structural Dynamics*. 2019;48(9):1045-1065.
36. Xu L H, Fan X W, Li Z X. Cyclic behavior and failure mechanism of self-centering energy dissipation braces with pre-pressed combination disc springs. *Earthquake Engineering & Structural Dynamics*. 2017;46(7):1065-1080.
37. Xu L H, Xie X S, Yao S Q, et al. Hysteretic behavior and failure mechanism of an assembled self-centering brace. *Bulletin of Earthquake Engineering*. 2019;17(6):3573-3592.
38. Kitayama S, Constantinou M C. Probabilistic collapse resistance and residual drift assessment of buildings with fluidic self-centering systems. *Earthquake Engineering & Structural Dynamics*. 2016;45(12):1935-1953.
39. Fang C, Zhong Q, Wang W, Hu S, Qiu C. Peak and residual responses of steel moment-resisting and braced frames under pulse-like near-fault earthquakes. *Engineering Structures*. 2018;177:579-597.
40. Qiu CX, Zhu S. High-mode effects on seismic performance of multi-story self-centering braced steel frames. *Journal of Constructional Steel Research.* 2016;119:133-143.
41. Bruneau M, MacRae G A. Reconstructing Christchurch: a seismic shift in building structural systems. *The Quake Centre, University of Canterbury, Christchurch*, 2017.
42. Karavasilis TL, Seo CY. Seismic structural and non-structural performance evaluation of highly damped self-centering and conventional systems. *Engineering Structures*. 2011;33(8):2248–2258.
43. Ray-Chaudhuri S, Hutchinson TC. Effect of nonlinearity of frame buildings on peak horizontal floor acceleration. *Journal of Earthquake Engineering*. 2011;15(1):124–142.
44. Hensher D A. Fiber-reinforced-plastic (FRP) reinforcement for concrete structures: properties and applications. *Elsevier*, 2016.
45. Banibayat P. Experimental investigation of the mechanical and creep rupture properties of basalt fiber reinforced polymer (BFRP) bars. *University of Akron*, 2011.
46. Attari N, Amziane S, Chemrouk M. Flexural strengthening of concrete beams using CFRP, GFRP and hybrid FRP sheets. *Construction and Building Materials*. 2012;37:746-757.
47. ASCE. *Minimum Design Loads for Buildings and other Structures. ASCE/SEI 7-16*. 2016.
48. Xu L, Fan X, Li Z. Experimental behavior and analysis of self-centering steel brace with pre-pressed disc springs. *Journal of Constructional Steel Research*. 2017;139:363-373.
49. Huang X, Eatherton MR, Zhou Z. Initial stiffness of self-centering systems and application to self-centering-beam moment-frames. *Engineering Structures*. 2020;203:109890.
50. Mazzoni S, McKenna F, Scott MH, Fenves GL. OpenSees command language manual. *Pacific Earthquake Engineering Research (PEER) Center*. 2006;264.
51. Baker J W. Quantitative classification of near-fault ground motions using wavelet analysis. *Bulletin of the Seismological Society of America.* 2007;97(5):1486-1501.
52. Somerville PG. Magnitude scaling of the near fault rupture directivity pulse. *Physics of the Earth and Planetary Interiors*. 2003;137:201–212.
53. FEMA. *FEMA P695: Quantification of building seismic performance factors*. 2009.

54. Fang C, Ping Y, Chen Y. Loading protocols for experimental seismic qualification of members in conventional and emerging steel frames. *Earthquake Engineering & Structural Dynamics*. 2020;49(2):155-174.
55. FEMA. *FEMA-350: Recommended seismic design criteria for new steel moment-frame buildings*. 2000.
56. FEMA. *FEMA-P58: Seismic performance assessment of buildings, volume I (Methodology)*. 2012.
57. Tremblay R, Lacerte M, Christopoulos C. Seismic response of multistory buildings with self-centering energy dissipative steel braces. *Journal of structural engineering*. 2008;134(1):108-120.
58. Vamvatsikos D, Cornell C A. Incremental dynamic analysis. *Earthquake engineering & structural dynamics*. 2002;31(3): 491-514.
59. U.S. Geological Survey. https://earthquake.usgs.gov/hazards/interactive/index.php [17 August 2020].